PCCP

PAPER

View Article Online
View Journal | View Issue

Cite this: *Phys. Chem. Chem. Phys.*, 2025, **27**, 17997

Molecular building-blocks for anion–π interactions

Élise Antonetti, Yoann Cotelle, Alexandre Martinez and Paola Nava *

Received 19th May 2025,
Accepted 27th July 2025

DOI: 10.1039/d5cp01879j

rsc.li/pccp

Theoretical calculations are performed to design a set of π molecules, significant for anion–π interactions. Quadrupole moments are reported at several levels of calculation. Trends from MP2 calculations are reproduced from DFT calculations, although actual values are different. Binding energies towards a chloride anion have been evaluated for the considered molecules and they roughly correlate with the quadrupole moment of the molecules, although other effects, such as structural flexibility, play a role. Imide moieties that decorate the π molecules provide privileged binding sites for anions; however, similar binding energies are obtained for the interaction between a chloride and benzenediimide, naphthalenediimide and perylenediimide, although quadrupole moments vary by a factor of two. The naphthalenediimide and the benzenetriimide emerge as valuable building blocks to construct extended molecular architectures with either C_2 or C_3 symmetry, for improved anion–π interactions and anion recognition.

1 Introduction

Anion–π interactions are non-covalent interactions that occur between negatively charged ions and electron-deficient π systems, showing a positive quadrupole moment. The first experimental evidence of their existence can be traced back to 2004,[1] although theoretical studies had already predicted their importance some years earlier.[2–4] Since then, anion–π interactions have attracted significant attention, as they have been shown to play a role in biological and chemical systems and in materials science.[5–13]

The nature of the anion–π interaction has been widely explored from theoretical and experimental points of view.[14–18] Early theoretical studies focus on the analysis of the interaction between anions and single-ring π systems, using various partition energy strategies, AIM (atoms in molecules) topological analysis, or electrostatic potential (ESP) maps.[10,16,19] Thus, substituted benzenes with electron-withdrawing groups,[3,4,20–22] as well as heterocycles or cyanuric acid derivatives,[2,14,23–25] have been identified as relevant molecular units. The anion–π interaction is predominantly due to electrostatic[22] and induction effects (anion-induced polarization of the π molecule)[20,24] and correlates with the quadrupole moment of the π molecule and its electrostatic potential.[26] The role of the substituents or heteroatoms in the π molecule has been highlighted by some authors: positive quadrupole moments and electrostatic potentials originate from the position of the nuclei, rather than from changes in the distribution of the π-electron density itself.[25,27] Other aspects can be mentioned, such as the direct interaction between local C–X dipoles (X being a substituent or heteroatom),[27] or orbital relaxation and possible charge transfer, notably in the case of anion–carbonyl interactions.[28] The anion also has an influence on the nature of the interaction: computational energy decomposition analysis (EDA) together with UV-vis and X-ray crystallographic experiments suggest that stabilization in anion–π complexes with fluoro- or oxoanions is prevalently related to electrostatic terms, while orbital relaxation is important for halide anions.[29]

Experimental works have demonstrated interest in combining extended π systems with high quadrupole moments, based for instance on the naphthalenediimide unit, to achieve effective anion–π interactions.[5,8,10] Within supramolecular chemistry, anion–π interactions can be then exploited to propose artificial systems for the recognition and transport of anions of biological or environmental interest.[5,8–10] For instance, the chloride anion plays an important role in biological processes (ion homeostasis, cell volume regulation, transepithelial transport, and regulation of electrical excitability) and several receptors have been reported for this anion.[8,30,31] Anion–π interactions could also contribute to the stabilization of reaction intermediates or transition states, thus playing a role in catalytic transformation.[11–13] As such, a comparative study of extended π-acidic surfaces is appealing.

The purpose of this work is to computationally predict a scale of increasing anion–π interactions, focusing on the design of π systems. We systematically treat planar π molecules of increasing size, from single-rings to extended systems. Therefore, we explore a variety of molecular platforms that possess

Aix Marseille Univ, CNRS, Centrale Med, iSm2, Marseille, France.
E-mail: paola.nava@univ-amu.fr

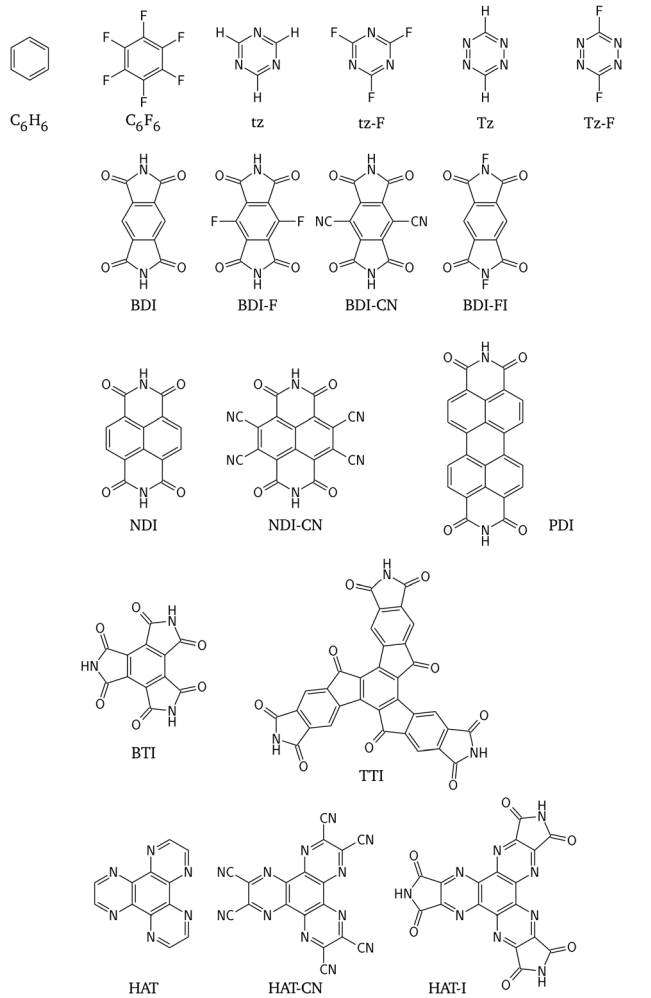

Fig. 1 Molecules treated in this work, and labels.

symmetry C_2 or C_3, which are potential candidates for the conception of elaborated molecular architectures. Our systematic approach is desirable and meaningful because it allows for direct comparison between the properties of the considered systems, all treated on the same footing. Starting from single-ring molecules (top of Fig. 1), extended π systems were constructed, which have been proven to be significant for anion–π interactions.[5,11] From the benzene ring, the benzenediimide molecule (BDI) is built formally by adding two cyclic imides. The BDI platform has been modified by introducing fluorine or cyano groups on the central ring or by modifying the imide moiety. The π system is further extended to obtain NDI- and PDI-based molecules (NDI = naphthalenediimide, PDI = perylenediimide). The benzenetriimide (BTI) is constructed by adding three cyclic imides to the central benzene, while the truxenonetriimide (TTI) contains three more extended π arms.[32] Finally, we considered systems derived from 1,4,5,8,9,12-hexaazatriphenylene (HAT).[33,34] For all of these molecules, quadrupole moments and polarizability values are provided, computed at several theoretical levels. We have then studied the interaction of these π molecules with a prototypical anion, the chloride. The binding energies and preferred binding sites are analyzed in light of the properties of isolated π molecules, by exploiting the electrostatic surface potential maps and computed charges.

2 Computational details

Density functional theory (DFT) and MP2 calculations were carried out using the TURBOMOLE program package.[35] The structures were optimized at each computational level in the gas phase.

MP2 calculations employ the aug-cc-pVTZ basis set and the corresponding auxiliary basis sets for the resolution of identity (RI) approximation.[36,37] Diffuse functions were omitted on hydrogen atoms (cc-pVTZ for H) for the TTI case,[38] to avoid convergence issues. In the case of small, single-ring molecules, CCSD(T) calculations were also performed to check polarizability values. For this purpose, the MOLPRO program package was used[39] and polarizabilities were computed numerically (see the SI for details on the basis set and polarizabilities).

For DFT calculations, the def2-TZVP basis set was employed throughout, together with the corresponding auxiliary basis sets for the RI technique.[40,41] Several functionals were tested for calculations of the quadrupole moments and polarizabilities of the molecules shown in Fig. 1: PBE0,[42–46] B3LYP,[42,43,47–50] CAM-B3LYP,[51] M06, M062X,[52] WB97XD[53] and SCLH22T.[54] For PBE0, B3LYP and CAM-B3LYP, the D3 empirical dispersion corrections were added.[55] Frequency calculations were performed on the PBE0-D3 structures to verify the nature of the stationary points, which are proved to be minima on their potential energy surface at this level of computation. In all cases, we report the Q_{zz} component of the quadrupole tensor, obtained by maintaining the π system in the *xy* plane.

Calculations of the interaction between the π systems and the chloride anion were performed at the levels of MP2, PBE0-D3 and SCLH22T only. Frequency calculations were performed on the PBE0-D3 adduct structures. The interaction is discussed in terms of binding energies ΔE, defined as follows:

$$\Delta E = E_{\pi\text{–Cl}^-} - E_{\pi} - E_{\text{Cl}^-} \quad (1)$$

where $E_{\pi\text{–Cl}^-}$, E_{π}, and E_{Cl^-} refer to the total electronic energies of the adduct, the isolated π system and the isolated chloride, respectively. The reported values ΔE are corrected for the basis set superposition error (BSSE) using the counterpoise method. Uncorrected results are available in the SI.

3 Results and discussion

3.1 Quadrupole moments and polarizabilities

Table 1 collects results from computed MP2 Q_{zz} values for all treated systems, as well as polarizabilities at the MP2 and CCSD(T) levels for single-ring molecules. Concerning quadrupole moments, our MP2 values are comparable to those reported in previous works at a similar level of computation: they are within 0.5 DÅ with respect to the MP2 values reported by Doerksen *et al.*,[56] employing a basis set optimized for

Table 1 Computed Q_{zz} (DÅ) values at the MP2/aug-cc-pVTZ level (unrelaxed values in parenthesis). Polarizabilities (a.u.) are reported at the MP2 and CCSD(T) levels. Selected values from previous contributions are reported, as well as experimental data, if available. Labels as in Fig. 1

	Q_{zz} (DÅ)		$\alpha_{\parallel}$ (a.u.)		
System	MP2	Lit.[a]	MP2	CCSD(T)	Lit.[a]
C_6H_6[b]	−7.97 (−8.71)	−7.99[56]	45.0	44.5	47.5[23]
tz[b]	0.84 (0.40)	0.90[14,56]	33.9	33.6	30.3[14]
Tz	3.31 (2.60)	3.32[56]	32.2	32.3	58.7[23]
C_6F_6[b]	8.04 (9.26)		42.5	42.2	
tz-F	8.07 (8.64)	8.23[14]	33.5	33.3	30.3[14]
Tz-F	8.28 (8.31)		32.2	32.3	
BDI	11.25 (14.23)				
BDI-F	14.73 (18.10)				
BDI-FI	23.19 (27.52)				
BDI-CN	24.39 (27.60)				
NDI	13.68 (16.67)	14.7[57]			
NDI-CN	53.17 (57.72)	55.5[58]			
PDI	21.00 (27.29)				
BTI	17.24 (21.52)	14.5[59]			
TTI[c]	36.25 (46.66)				
HAT	−8.79 (−10.72)	−8.53[16]			54.0[16]
HAT-I	27.04 (34.95)				
HAT-CN	75.12 (80.10)				

[a] Computational levels: ref. 56: MP2/[5s3p2d/3s2p]//MP2/6-31G(d); ref. 14: MP2/6-31G* for Q_{zz} and MP2/6-31++G** for $\alpha_{\parallel}$; ref. 57 and 58: MP2/6-311G**//PBE0/6-311++G**; ref. 23: MP2/6-311+G**. [b] Exp. Q_{zz} for C_6H_6: −8.69 ± 0.5, gas phase;[60] −8.48 ± 0.36, in CCl_4.[61] For tz: −0.83 ± 0.93 in C_6H_{12};[62] −1.05 ± 0.17 from X-ray.[63] For C_6F_6: 9.5 ± 0.5, gas phase.[60] [c] cc-pVTZ basis for H atoms.

polarizabilities; they are within 2 DÅ with respect to the values from experiments. The largest discrepancy is for the BTI system,[59] but we believe that the reported value was not computed at the MP2 level. DFT results are reported in Fig. 2 and Table 2. The computed unsigned values are systematically lower than those obtained at the MP2 level. However, and satisfactorily, the DFT methods reproduce the MP2 trends, as visualized by the regression line in Fig. 2 for PBE0-D3 (R^2 = 0.9996). Similar behaviors are observed for the other functionals, as detailed in Table 2: R^2 values are always larger than 0.997.

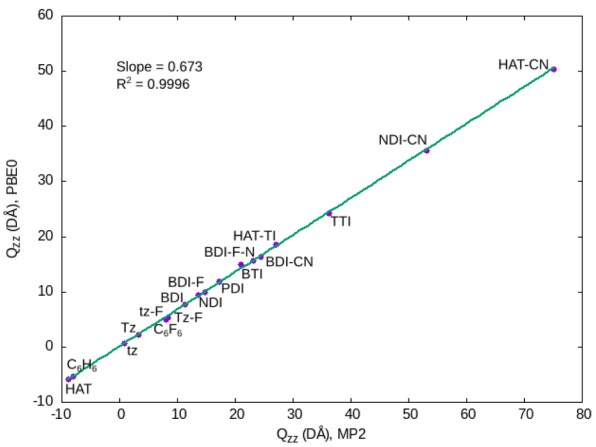

Fig. 2 Correlation curve between quadrupole moments Q_{zz} (DÅ) computed at the MP2 and PBE0-D3 levels. Labels for molecules as in Fig. 1.

Expanding the benzene ring to BDI, thus adding cyclic imides, has a large effect on Q_{zz}, which increases from −7.97 (benzene) to 11.25 DÅ (BDI, MP2 values). Substitutions on the BDI have also an impact: the quadrupole moment increases by 3.5 DÅ by replacing the hydrogen by fluorine atoms on the central 6-membered ring. Interestingly, the Q_{zz} values become more than twice larger, either by introducing cyano groups on the central ring, or by modifying N–H to N–F in the imide moiety. The extension of the aromatic core from BDI to NDI increases the Q_{zz} value only slightly. The increase is more pronounced for PDI, with a value of Q_{zz} close to that of BDI-CN. Again, and as expected,[5,11] the effect of the cyano substitution is evident when comparing NDI and NDI-CN. The computed quadrupole moment of the NDI-CN (MP2: 53.17 DÅ) is comparable to the previously reported value for a similar structure (55.5 DÅ computed for an N-substituted tetracianoNDI).[58]

A value of Q_{zz} of 17.24 DÅ (MP2 value) is associated with the BTI molecule, which contains three cyclic imide moieties, and thus is higher than the value obtained for BDI. The value of Q_{zz} increases considerably to 36.25 DÅ for the TTI molecule. The HAT system has a negative Q_{zz}. By decorating it with three cyclic imide moieties or cyano groups, positive Q_{zz} values are obtained.

Concerning polarizabilities,[14,16,23] MP2 values for small systems are the same as those obtained at the CCSD(T) level (within 0.5 a.u.), Table 1. The values obtained from DFT (PBE0-D3), Table 2, are underestimated, but trends are respected. Previously, it has been argued that the *s*-tetrazine has a significant larger polarizability than benzene (58.7 a.u. and 47.5 a.u., respectively at the MP2 level).[23] However, from high accurate CCSD(T) calculations we conclude that benzene has the largest polarizability (44.5 a.u.) among the six single-ring molecules studied and that the *s*-tetrazine has a similar polarizability to *s*-triazine (32.3 a.u. and 33.6, respectively), thus lower than that of benzene, Table 1. Fluorine substitution has no impact on polarizabilities; however, Tables 1 and 2, while introducing cyano groups increases them slightly. The effect is much larger when imide groups are introduced (DFT values, Table 2), as can be seen by comparing benzene (38.60 a.u.) to BDI (63.75 a.u.), BDI to BTI (76.19 a.u.), or HAT (79.93 a.u.) to HAT-I (118.23 a.u.). Finally, extending the π system from BDI to HAT and then to NDI, PDI and TTI has the greatest effect on polarizability, which then rises up to 172.4 a.u. (PBE0-D3) for TTI, Table 2.

3.2 Interaction with an anion

To go a step further, the structures of the adducts between the considered π molecules and the chloride were optimized to evaluate the binding energies and correlate them with the calculated quadrupole moments of the π molecules. Moreover, although the computed positive values Q_{zz} suggest favorable interactions with anions, they do not provide information about the preferred binding sites. For small molecules, from benzene to difluoro-*s*-tetrazine, the chloride has been forced to be on the *Oz* axis, to avoid other interactions, *i.e.* hydrogen

Table 2 Q_{zz} (DÅ) values obtained at several DFT levels of calculation, def2-TZVP basis set. Intercept, slope and R^2 from the linear regression with relaxed-MP2 values for Q_{zz} are indicated, as for PBE0-D3 in Fig. 2. Polarizabilities (a.u.) are reported at the PBE0-D3 level. Labels are as given in Fig. 1

	Q_{zz} (DÅ)							$\alpha_{\parallel}$ (a.u.)
System	PBE0-D3	M06	M062X	WB97XD	CAM-B3LYP-D3	B3LYP	SCLH22T	PBE0-D3
C_6H_6	−5.43	−4.94	−5.48	−5.41	−5.26	−5.26	−5.27	38.60
tz	0.58	0.87	0.48	0.61	0.72	0.74	0.70	29.71
Tz	2.14	2.34	2.04	2.17	2.28	2.29	2.27	28.49
C_6F_6	4.92	5.29	5.31	5.17	5.69	5.55	5.72	38.17
tz-F	5.18	5.30	5.38	5.27	5.58	5.52	5.64	29.36
Tz-F	5.35	5.45	5.44	5.43	5.69	5.61	5.72	28.53
BDI	7.65	8.20	7.64	7.88	8.54	8.49	8.38	63.75
BDI-F	9.95	10.54	10.00	10.23	10.96	10.84	10.76	63.78
BDI-FI	15.64	16.47	16.02	16.10	16.96	16.73	16.87	64.02
BDI-CN	16.39	17.04	16.29	16.80	17.63	17.36	17.36	75.60
NDI	9.37	10.28	9.23	9.57	10.42	10.55	10.18	81.48
NDI-CN	35.65	36.75	35.62	36.50	37.74	37.20	37.35	105.25
PDI	14.95	16.45	14.39	14.97	16.53	17.15	16.24	125.48
BTI	11.80	12.46	11.76	12.16	13.04	12.85	12.78	76.19
TTI	24.16	25.92	24.30	25.04	27.47	27.22	26.45	172.43
HAT	−5.84	−4.55	−6.38	−5.86	−5.40	−5.08	−5.84	79.93
HAT-I	18.50	19.69	18.57	18.97	20.54	20.25	19.97	118.23
HAT-CN	50.43	51.55	50.34	51.53	52.74	51.82	52.36	116.56
Intercept	0.010	0.562	−0.038	0.058	0.524	0.625	0.407	
Slope	0.673	0.684	0.674	0.688	0.707	0.695	0.700	
R^2	0.9996	0.9981	0.9998	0.9997	0.9981	0.9971	0.9990	

Table 3 MP2, PBE0-D3 and SCLH22T binding energies of the chloride, ΔE (kJ mol^{-1}), as defined in eqn (1). D3 empirical dispersion parameters were employed for PBE0 calculations. The binding sites are denoted as s_A (imide site), s_B (TTI case) and s_C (central ring), Fig. 3

Complex	Site	MP2	PBE0-D3	SCLH22T
C_6H_6	s_C[a]	1.6	8.4	8.4
tz	s_C[a]	−32.5	−27.7	−26.5
Tz	s_C[a]	−45.3	−40.4	−39.0
C_6F_6	s_C	−62.0	−55.3	−57.4
tz-F	s_C	−72.2	−67.9	−68.9
Tz-F	s_C[a]	−75.4	−69.0	−70.3
BDI	s_A	−86.3	−91.1	−85.3
BDI-F	s_A	−102.2	−108.9	−104.1
BDI-FI	s_A	−118.9	−123.0	−118.4
BDI-CN	s_A	−136.8	−147.3	−140.6
NDI	s_A	−91.6	−94.3	−87.7
NDI-CN	s_A	−185.3	−200.4	−191.9
PDI	s_C	−90.7	−91.1	−81.7
PDI	s_A	−85.5	−91.3	−82.1
BTI	s_A	−112.6	−119.2	−111.9
TTI	s_B	−150.5	−151.3	−144.0
TTI	s_A	−97.2	−113.9	−105.2
TTI[a]	s_C[a]	−122.0	−111.1	−104.3
HAT	s_C	−65.1	−58.1	−49.4
HAT-I	s_A	−152.2	−153.0	−144.0
HAT-I	s_C	−135.7	−143.0	−133.5
HAT-CN	s_C	−216.0	−222.5	−215.4

[a] Imaginary frequencies due to imposed constraints.

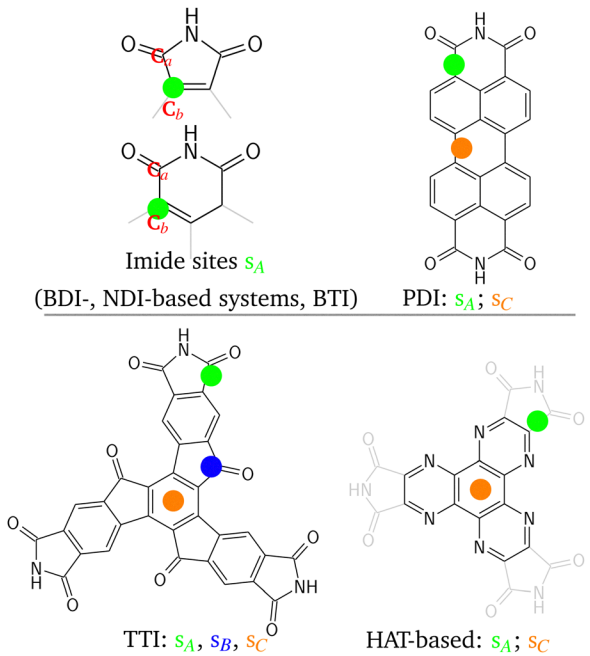

Fig. 3 Top view of the chloride binding sites. Green circles indicate positions close to the imide (s_A), orange circles are on the most central rings (s_C), and the blue circle indicates a site close to the cyclopentenone moiety (s_B).

bonding. In some cases, due to the applied constraints, imaginary frequencies appear, Table 3.

For π systems containing fused rings, several structures were fully optimized to identify anion binding sites, Fig. 3 and Table 3. The chloride was approached along the z axis, *e.g.* from above the π system, to avoid structures in which the anion interacts with a hydrogen atom in the molecular plane. In most cases, the preferred (and sometimes unique) binding site is on top of the imide unit, usually displaced to the C_a–C_b bond, where C_a is the carbon atom of the carbonyl moiety (green sites, s_A, Fig. 3): BDI-based systems, NDI-based systems, BTI and HAT-I. In the case of the PDI platform, we identify two sites that lead to very close ΔE: in addition to the site close to the imide (s_A in green, ΔE = −85.5 kJ mol^{-1}), a second binding site leads to an adduct with a ΔE = −90.7 kJ mol^{-1} (s_C in orange, MP2 values). For the TTI molecule we investigated three

possibilities: the site close to the imide (s_A in green, MP2 ΔE = −97.2 kJ mol^{-1}); the site close to the cyclopentenone moiety (s_B in blue, MP2 ΔE = −150.5 kJ mol^{-1}); finally, the approach on the C_3 axis was also calculated (s_C in orange, MP2 ΔE = −122.0 kJ mol^{-1}). In the case of the HAT-based derivatives, a site on the central ring was obtained, and, in the case of the HAT-I platform, the imide position was retrieved as well.

Interestingly, the binding sites are consistent with the results from both the NBO and Hirshfeld charges, and the ESP maps, evaluated for isolated π molecules, and shown for the BDI, TTI and HAT cases in Fig. 4. Accordingly, the carbon atoms with the highest computed charges are those close to the imide moieties for BDI. For the TTI system, two sites emerge, *e.g.* close either to the imide or to the carbonyl of the cyclopentenone. The full data for all treated molecules are available in the SI.

Concerning methods, the MP2 trends on ΔE are reproduced by the DFT approaches, as shown by the regression lines in the SI (R^2 = 0.987 for both PBE0-D3 and SCLH22T). We notice that the PBE0-D3 values for the s_C sites are often slightly larger, while the PBE0-D3 methods usually overstabilize the complexes at the imide sites s_A with respect to MP2. Consequently, the PBE0-D3 calculated distances for Cl–C_a and Cl–C_b are significantly shorter than in MP2, Table 4. In apparent contrast with our results, previous reports show that DFT provides longer distances and lower stabilization energies (in absolute value) than MP2. This difference is due to the fact that we included dispersion corrections in our DFT calculations, which contribute to the stabilization of the anion–π complexes.[3,10]

Table 4 MP2 and PBE0-D3 computed distances (pm) between the chloride and the carbon atoms close to the imide binding sites, Fig. 3

	MP2		PBE0-D3	
System	Cl–C_a	Cl–C_b	Cl–C_a	Cl–C_b
BDI	294.06	292.11	278.10	278.13
BDI-F	287.16	278.19	279.02	269.73
BDI-FI	275.07	278.35	270.77	268.61
BDI-CN	279.95	258.03	276.80	253.64
NDI	313.82	309.43	283.37	280.61
NDI-CN	279.19	245.61	275.42	239.25
PDI	304.91	297.54	285.09	276.75
BTI	289.89	269.44	282.36	262.84
TTI	286.36	274.81	279.22	259.28
HAT-I	282.04	244.45	278.36	242.40

The plot in Fig. 5 collects the MP2 computed values ΔE for the most stable adducts as a function of the Q_{zz} of the corresponding π systems. The interaction between the anion and the π molecule roughly follows the quadrupole moment, as the values of ΔE decrease with increasing Q_{zz}. However, the regression line with an R^2 = 0.877, lower than 0.95, suggests that the quadrupole moment is not the only factor that affects the binding energies and prompted us to further analyze the computed data.

First of all, the HAT molecule has a remarkably low ΔE, despite its negative Q_{zz}. This can be understood by inspecting the ESP map, Fig. 4, which reveals that the electrostatic potential is positive on the carbon atoms of the central ring and associated charges are also positive.

Let us now focus on the systems where the anion approaches from the top of the imide sites (s_A, green cases in Fig. 5). From

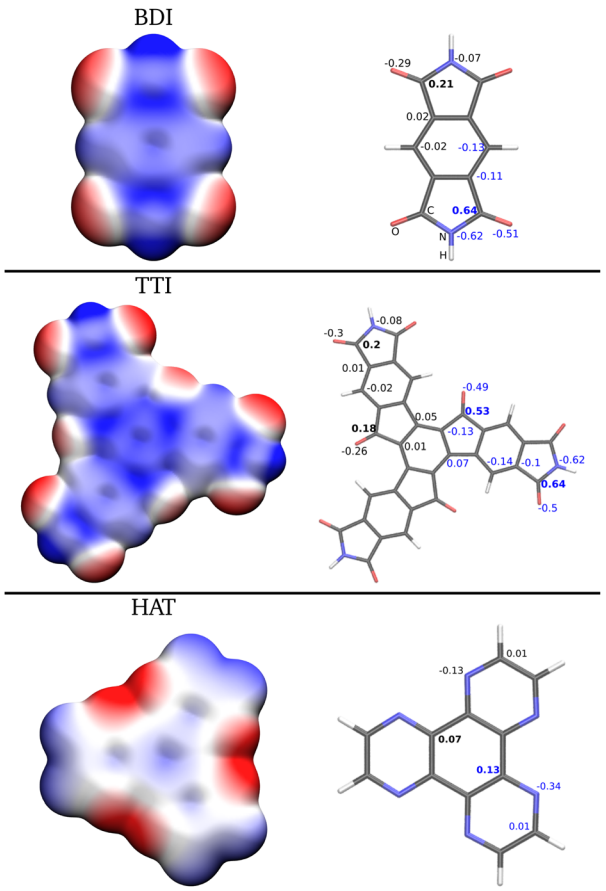

Fig. 4 Electrostatic potential maps for selected π systems, mapped on the electron density iso-surface of 0.001 a.u. The red color corresponds to a negative region of the electrostatic potential (−0.04 a.u.), whereas the blue color corresponds to the region where the potential is positive (+0.04 a.u.). Charges (NBO in blue and Hirshfeld in black) are indicated for heteroatoms.

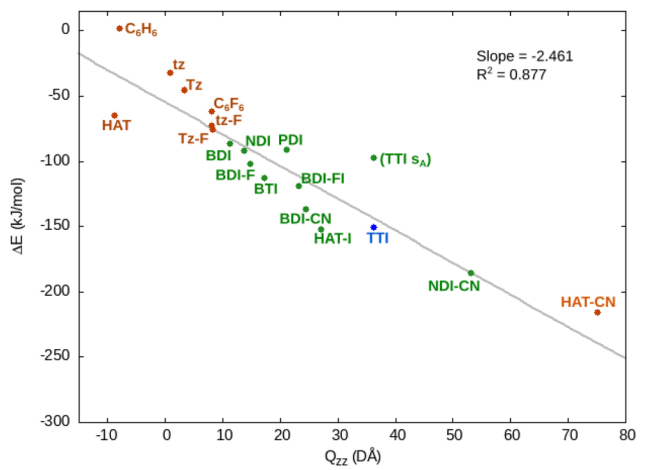

Fig. 5 Smallest MP2 computed ΔE values (among the tested adduct structures) as a function of the Q_{zz} of each π system. Orange, green and blue dots refer to s_C, s_A and s_B binding sites, as in Fig. 3. The value for the TTI s_A case is also reported (but not used for the regression).

the point of view of the structures, the MP2 distances between the chloride anion and carbon atoms C_a and C_b vary between 244 and 314 pm and are sensitive to substitutions, Table 4. The Cl–C_b distances are usually shorter than the corresponding Cl–C_a distances, indicating that the anion position is slightly displaced toward the C_b atom. In this way, repulsive interactions between the anion and the nitrogen or oxygen atoms of the imide moiety are minimized. The Cl–C_a distance becomes shorter when NDI and NDI-CN are compared, or within the BDI, BDI-F and BDI-CN series. Substitution with the electron-withdrawing group (–CN or –F) is performed in the β position: it affects the strength of the interaction, but the electron-withdrawing group is sufficiently far from C_a, and repulsion with the incoming anion is therefore avoided. Thus, when comparing NDI and NDI-CN, Q_{zz} increases and ΔE decreases. Again, within the series BDI, BDI-F and BDI-CN (substitutions with electron-withdrawing groups), the Q_{zz} values increase and the ΔE values decrease. Similarly, ΔE decreases from BDI to BTI (from two to three imide moieties). However, and interestingly, the binding energies are close for BDI, NDI, and PDI, although the PDI molecule has a significantly larger quadrupole moment. In addition, there is no improvement for the TTI (s_A site) compared to the BTI.

The TTI system is instructive: the preferred binding site is close to the ketone in the cyclopentenone (blue site in Fig. 3, s_B), although the calculated charge is slightly higher for the carbon atom in the imide moiety, Fig. 4. Inspection of the PBE0-D3 adduct geometries, Fig. 6, reveals that the Cl–C_a distance in s_A (279 pm) is significantly longer than Cl–C_2 in s_B (252 pm) and that there is more structural flexibility close to the binding site in s_B than in s_A. Approaching the anion causes a distortion in the planarity of the π molecule, which is more significant for the s_B adduct. It could be argued that the binding energy results from the modification of the π system, meaning that it would essentially be due to the negative charge interacting with the induced dipole moment of the modified π system. Yet, the dipole moments of the neutral π molecules in the geometry of the chloride adducts, Table 5 for TTI and BDI, are quite small, although the values for TTI site s_B are, as expected, slightly higher (dipole moment values for all π systems are available in the SI). We then evaluated the binding energies for adducts, where we constrained the planarity of the binding site.

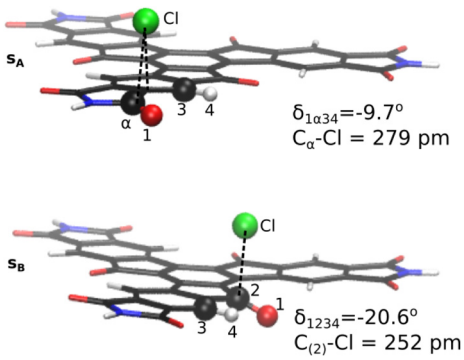

Fig. 6 PBE0-D3 optimized structures of the adduct between the chloride and the TTI molecule, sites s_A and s_B.

Table 5 Dipole moments (*D*) of the neutral π molecules in the geometry of the unconstrained adducts (left) and the adducts with constrained planarity (right). PBE0-D3 binding energies are also reported (kJ mol^{-1})

	Unconstrained adduct		Adduct with constrained planarity	
System	ΔE	Dipole	ΔE	Dipole
BDI	−91.1	0.54	−84.4	0.07
TTI s_A	−113.9	0.46	−107.1	0.10
TTI s_B	−151.3	0.67	−140.6	0.19

In all cases, the so-obtained binding energies are only up to 11 kJ mol^{-1} higher than in the optimized structures, and the global gain in energy from the anion–dipole interaction that compensates for the deformation of the π structure is rather small. Finally, energy decomposition analysis (EDA) was used to compare the s_B and s_A adducts, Fig. 7. This analysis was also performed on a structure where the Cl–C_a distance is shortened up to 252 pm (s_A(252) structure in Fig. 7), which is the Cl–C_2 distance in s_B (results of further constrained structures are collected in the SI). In this approach, the interaction energy ΔE is decomposed into several contributions: $\Delta E = E_{exc\text{-}rep} + E_{elec} + E_{or} + E_{corr} + E_{disp}$. Stabilizing contributions from correlation (E_{corr}) and dispersion (E_{disp}) terms are similar in all cases. The favorable binding energies ΔE originate primarily from the compensation between positive repulsive contributions ($E_{exc\text{-}rep}$) on the one side and negative electrostatic (E_{elec}) and orbital relaxation (E_{or}) contributions on the other side. By approaching the chlorine anion towards the C_a atom, we recover the same electrostatic and orbital relaxation terms as in the s_B adduct, but the repulsion contribution has clearly increased. This suggests that the approach of the anion at the s_A site is somewhat limited by the structural rigidity of the imide moiety and the repulsive interactions that arise. Thus, the more favorable ΔE calculated for the site s_B than s_A results from structural flexibility and from the fact that repulsive interactions in s_A prevent the anion from getting close to the C_a atom.

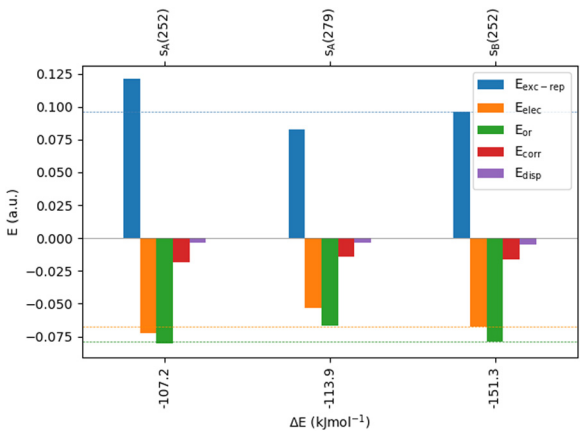

Fig. 7 Energy decomposition analysis performed on the PBE0-D3 optimized structures of the adduct between a chloride and the TTI molecule, sites s_A and s_B, denoted s_A(279) and s_B(252). In the s_A(252) structure the Cl–C_a distance is 252 pm. The terms of the decomposition are given in the main text.

4 Conclusions

In the present study, we report a comprehensive and systematic study of π molecules significant for anion–π interactions.

First, we report a corrected value for the polarizability of the *s*-tetrazine ($\alpha_{\parallel}$ = 32.3 a.u., CCSD(T) level). Concerning quadrupole moments, we show that DFT calculations with a set of def2-TZVP bases provide correct trends compared to MP2-computed reference results, although absolute values may differ significantly. Thus, care should be taken when comparing computed quadrupole moments from different sources if the methods used are not the same or if the computational levels are unclear. Moreover, we establish a linear relationship between MP2 and DFT results. This suggests that, by providing the coefficients of the regression line, quadrupole moments of MP2 quality can be extrapolated from a simple DFT run, thus avoiding the actual MP2 calculation, the convergence of which is tedious for extended systems together with diffuse basis functions.

The interaction between a chloride anion and π molecules has been investigated by evaluating the binding energies. Computed charges and ESP maps are convenient tools for predicting possible binding sites of an anion on a neutral molecular structure, and they could be particularly useful when dealing with extended, non-planar molecules. As expected, the binding energies decrease roughly with the quadrupole moments of the π molecules. However, equilibrium geometries and binding energies result from a compromise between several factors, including local structural rigidity. Interestingly, imide moieties provide privileged binding sites for anions, but BDI, NDI, and PDI, or BTI and TTI display similar binding energies (on the imide binding site), although the quadrupole moments are different. The binding energy clearly decreases by performing a β-substitution on the imide carbon atom, such as for BDI-CN in comparison to BDI. Alternatively, the decrease in binding energy is evident when BDI is compared to BTI, thus introducing another imide moiety on the π platform.

In the case of the TTI molecule, three binding sites have been evaluated. The most favorable site, s_B, is close to the carbonyl moiety near the central ring. It offers more structural flexibility and less repulsive interactions than the s_A site. These aspects – structural flexibility and repulsive interactions between the incoming anion and heteroatoms – also emerge as factors that affect the anion–π interaction strength.

Finally, the π platforms that are presented in this study are suitable to promote anion–π interactions. Among them, NDI emerges as a privileged choice to conceive extended molecular architectures with C_2 symmetry, for improved anion–π interactions and anion recognition. Similarly, BTI turns out to be the best candidate as a C_3-symmetry building block. In fact, it has recently been used to synthesize molecular cages that combine such a platform with an electron-rich cyclotriveratrylene (CTV).[64,65] The TTI molecule remains an attractive alternative that offers a more extended structural core than BTI.

Conflicts of interest

There are no conflicts to declare.

Data availability

Details of MP2 and CCSD(T) calculations, computed binding energies, details of structural parameters, EDA on TTI structures, all ESP maps and charges, coordinates. See DOI: **https://doi.org/10.1039/d5cp01879j**

The data supporting this article have been included as part of the SI.

Acknowledgements

This study was carried out with financial support from the Agence Nationale de la Recherche (ANR-19-CE07-0024 and ANR-21-CE07-0011).

Notes and references

1 P. de Hoog, P. Gamez, I. Mutikainen, U. Turpeinen and J. Reedijk, *Angew. Chem.*, 2004, **116**, 5939–5941.
2 M. Mascal, A. Armstrong and M. D. Bartberger, *J. Am. Chem. Soc.*, 2002, **124**, 6274–6276.
3 I. Alkorta, I. Rozas and J. Elguero, *J. Am. Chem. Soc.*, 2002, **124**, 8593–8598.
4 D. Quiñonero, C. Garau, C. Rotger, A. Frontera, P. Ballester, A. Costa and P. M. Deyà, *Angew. Chem., Int. Ed.*, 2002, **41**, 3389–3392.
5 R. E. Dawson, A. Hennig, D. P. Weimann, D. Emery, V. Ravikumar, J. Montenegro, T. Takeuchi, S. Gabutti, M. Mayor, J. Mareda, C. A. Schalley and S. Matile, *Nat. Chem.*, 2010, **2**, 533–538.
6 X. Lucas, A. Bauzá, A. Frontera and D. Quiñonero, *Chem. Sci.*, 2016, **7**, 1038–1050.
7 Z. Huang, Y. Bai, X. Huang, J. Li, Y. Wu, Y. Chen, K. Li, X. Niu, N. Li, G. Liu, Y. Zhang, H. Zai, Q. Chen, T. Lei, L. Wang and H. Zhou, *Nature*, 2023, **623**, 531–537.
8 V. Gorteau, G. Bollot, J. Mareda, A. Perez-Velasco and S. Matile, *J. Am. Chem. Soc.*, 2006, **128**, 14788–14789.
9 Z. Xu, N. J. Singh, S. K. Kim, D. R. Spring, K. S. Kim and J. Yoon, *Chem. – Eur. J.*, 2011, **17**, 1163–1170.
10 I. A. Rather, S. A. Wagay and R. Ali, *Coord. Chem. Rev.*, 2020, **415**, 213327.
11 C. Wang, F. N. Miros, J. Mareda, N. Sakai and S. Matile, *Angew. Chem., Int. Ed.*, 2016, **55**, 14422–14426.
12 A.-B. Bornhof, A. Bauzá, A. Aster, M. Pupier, A. Frontera, E. Vauthey, N. Sakai and S. Matile, *J. Am. Chem. Soc.*, 2018, **140**, 4884–4892.
13 Y. Zhao, Y. Domoto, E. Orentas, C. Beuchat, D. Emery, J. Mareda, N. Sakai and S. Matile, *Angew. Chem., Int. Ed.*, 2013, **52**, 9940–9943.
14 C. Garau, A. Frontera, D. Quiñonero, P. Ballester, A. Costa and P. M. Deyà, *ChemPhysChem*, 2003, **4**, 1344–1348.
15 D. Y. Kim, N. J. Singh, J. W. Lee and K. S. Kim, *J. Chem. Theory Comput.*, 2008, **4**, 1162–1169.
16 B. L. Schottel, H. T. Chifotides and K. R. Dunbar, *Chem. Soc. Rev.*, 2007, **37**, 68–83.

17 A. Frontera, P. Gamez, M. Mascal, T. J. Mooibroek and J. Reedijk, *Angew. Chem., Int. Ed.*, 2011, **50**, 9564–9583.
18 S. V. Rosokha, *ChemPlusChem*, 2023, **88**, e202300350.
19 O. Zayene, R. Plais, L. Rolhion, F. Bourdreux, G. Pieters, A. Gaucher, G. Clavier, A. Cœuret, J.-Y. Salpin and D. Prim, *ChemistrySelect*, 2024, **9**, e202302763.
20 D. Kim, P. Tarakeshwar and K. S. Kim, *J. Phys. Chem. A*, 2004, **108**, 1250–1258.
21 D. Y. Kim, N. J. Singh and K. S. Kim, *J. Chem. Theory Comput.*, 2008, **4**, 1401–1407.
22 J. Thirman and M. Head-Gordon, *J. Phys. Chem. A*, 2017, **121**, 717–728.
23 C. Garau, D. Quiñonero, A. Frontera, A. Costa, P. Ballester and P. M. Deyà, *Chem. Phys. Lett.*, 2003, **370**, 7–13.
24 A. Frontera, F. Saczewski, M. Gdaniec, E. Dziemidowicz-Borys, A. Kurland, P. M. Deyà, D. Quiñonero and C. Garau, *Chem. – Eur. J.*, 2005, **11**, 6560–6567.
25 S. E. Wheeler and J. W. G. Bloom, *Chem. Commun.*, 2014, **50**, 11118–11121.
26 A. Bauzá, D. Quiñonero, P. M. Deyà and A. Frontera, *Chem. Phys. Lett.*, 2013, **567**, 60–65.
27 S. E. Wheeler and K. N. Houk, *J. Phys. Chem. A*, 2010, **114**, 8658–8664.
28 J. Zhu, D.-H. Tuo, X.-D. Wang, Y.-F. Ao, Q.-Q. Wang and D.-X. Wang, *Org. Lett.*, 2024, **26**(28), 5984–5988.
29 F. E. Odubo, M. Zeller and S. V. Rosokha, *J. Phys. Chem. A*, 2023, **127**, 5851–5859.
30 T. J. Jentsch, V. Stein, F. Weinreich and A. A. Zdebik, *Physiol. Rev.*, 2002, **82**, 503–568.
31 G. Gil-Ramírez, E. C. Escudero-Adán, J. Benet-Buchholz and P. Ballester, *Angew. Chem.*, 2008, **120**, 4182–4186.
32 S. Kumar, Y. H. Koo, T. Higashino, W. Matsuda, S. Ghosh, Y. Tsutsui, M. Suda, H. Imahori, K. Suzuki, H. Kaji and S. Seki, *Adv. Electron. Mater.*, 2022, **8**, 2101390.
33 H. T. Chifotides, B. L. Schottel and K. R. Dunbar, *Angew. Chem.*, 2010, **122**, 7360–7365.
34 G. Aragay, A. Frontera, V. Lloveras, J. Vidal-Gancedo and P. Ballester, *J. Am. Chem. Soc.*, 2013, **135**, 2620–2627.
35 *TURBOMOLE V7.5 2020 and V7.8 2024 (for SCLH22T), a development of University of Karlsruhe and Forschungszentrum Karlsruhe GmbH, 1989–2007*, TURBOMOLE GmbH, since 2007; available from **https://www.turbomole.org**.
36 R. A. Kendall, T. H. Dunning, Jr. and R. J. Harrison, *J. Chem. Phys.*, 1992, **96**, 6796–6806.
37 F. Weigend, A. Köhn and C. Hättig, *J. Chem. Phys.*, 2002, **116**, 3175–3183.
38 T. H. Dunning, Jr., *J. Chem. Phys.*, 1989, **90**, 1007–1023.
39 H.-J. Werner, P. J. Knowles, G. Knizia, F. R. Manby, M. Schütz, P. Celani, W. Györffy, D. Kats, T. Korona, R. Lindh, A. Mitrushenkov, G. Rauhut, K. R. Shamasundar, T. B. Adler, R. D. Amos, S. J. Bennie, A. Bernhardsson, A. Berning, D. L. Cooper, M. J. O. Deegan, A. J. Dobbyn, F. Eckert, E. Goll, C. Hampel, A. Hesselmann, G. Hetzer, T. Hrenar, G. Jansen, C. Köppl, S. J. R. Lee, Y. Liu, A. W. Lloyd, Q. Ma, R. A. Mata, A. J. May, S. J. McNicholas, W. Meyer, T. F. M. III, M. E. Mura, A. Nicklass, D. P. O'Neill, P. Palmieri, D. Peng, K. Pflüger, R. Pitzer, M. Reiher, T. Shiozaki, H. Stoll, A. J. Stone, R. Tarroni, T. Thorsteinsson, M. Wang and M. Welborn, *MOLPRO, version 2021, a package of ab initio programs*, see **https://www.molpro.net**.
40 F. Weigend and R. Ahlrichs, *Phys. Chem. Chem. Phys.*, 2005, **7**, 3297–3305.
41 F. Weigend, *Phys. Chem. Chem. Phys.*, 2006, **8**, 1057–1065.
42 P. A. M. Dirac and R. H. Fowler, *Proc. R. Soc. London*, 1929, **123**, 714–733.
43 J. C. Slater, *Phys. Rev.*, 1951, **81**, 385–390.
44 J. P. Perdew and Y. Wang, *Phys. Rev. B:Condens. Matter Mater. Phys.*, 1992, **45**, 13244–13249.
45 J. P. Perdew, K. Burke and M. Ernzerhof, *Phys. Rev. Lett.*, 1996, **77**, 3865–3868.
46 J. P. Perdew, M. Ernzerhof and K. Burke, *J. Chem. Phys.*, 1996, **105**, 9982–9985.
47 S. Vosko, L. Wilk and M. Nussair, *Can. J. Phys.*, 1980, **58**, 1200.
48 A. D. Becke, *Phys. Rev. A:At., Mol., Opt. Phys.*, 1988, **38**, 3098–3100.
49 C. Lee, W. Yang and R. G. Parr, *Phys. Rev. B:Condens. Matter Mater. Phys.*, 1988, **37**, 785.
50 A. D. Becke, *J. Chem. Phys.*, 1993, **98**, 5648–5652.
51 T. Yanai, D. P. Tew and N. C. Handy, *Chem. Phys. Lett.*, 2004, **393**, 51–57.
52 Y. Zhao and D. G. Truhlar, *Theor. Chem. Acc.*, 2008, **120**, 215–241.
53 J.-D. Chai and M. Head-Gordon, *Phys. Chem. Chem. Phys.*, 2008, **10**, 6615.
54 A. Wodyński and M. Kaupp, *J. Chem. Theory Comput.*, 2022, **18**, 6111–6123.
55 S. Grimme, J. Antony, S. Ehrlich and H. Krieg, *J. Chem. Phys.*, 2010, **132**, 154104.
56 R. J. Doerksen and A. J. Thakkar, *J. Phys. Chem. A*, 1999, **103**, 10009–10014.
57 V. Gorteau, G. Bollot, J. Mareda and S. Matile, *Org. Biomol. Chem.*, 2007, **5**, 3000.
58 J. Mareda and S. Matile, *Chem. – Eur. J.*, 2009, **15**, 28–37.
59 D.-H. Tuo, Y.-F. Ao, Q.-Q. Wang and D.-X. Wang, *Org. Lett.*, 2019, **21**, 7158–7162.
60 M. R. Battaglia, A. D. Buckingham and J. H. Williams, *Chem. Phys. Lett.*, 1981, **78**, 421–423.
61 G. R. Dennis and G. L. D. Ritchie, *J. Phys. Chem.*, 1991, **95**, 656–660.
62 I. C. Walker, M. H. Palmer and C. C. Ballard, *Chem. Phys.*, 1992, **167**, 61–75.
63 M. A. Spackman, *Chem. Rev.*, 1992, **92**, 1769–1797.
64 L. Miton, E. Antonetti, D. García-López, P. Nava, V. Robert, M. Albalat, N. Vanthuyne, A. Martinez and Y. Cotelle, *Chem. – Eur. J.*, 2024, **30**, e202303294.
65 L. Miton, P.-A. Dupin, E. Antonetti, M. Jean, P. Nava, A. Martinez and Y. Cotelle, *Org. Biomol. Chem.*, 2025, **23**, 4360–4364.

